10-1-2013

Electron Transfer Precedes ATP Hydrolysis during Nitrogenase Catalysis

Simon Duval
Utah State University

Karamatullah Danyal
Utah State University

Sudipta Shaw
Utah State University

Anna K. Lytle
Utah State University

Dennis R. Dean
Virginia Polytechnic Institute and State University

See next page for additional authors

Accepted version. *Proceedings of the National Academy of Sciences*, Vol. 110, No. 41 (October 2013): 16414-16419. DOI.
Edwin Antony was affiliated with Utah State University at the time of publication.

Electron Transfer Precedes ATP Hydrolysis During Nitrogenase Catalysis

Simon Duval
Department of Chemistry and Biochemistry
Utah State University
Logan, UT
Karamatullah Danyal
Department of Chemistry and Biochemistry
Utah State University
Logan, UT
Sudipta Shaw
Department of Chemistry and Biochemistry
Utah State University
Logan, UT
Anna K. Lytle
Department of Chemistry and Biochemistry
Utah State University
Logan, UT
Dennis R. Dean
Department of Biochemistry
Virginia Polytechnic Institute and State University
Blacksburg, VA

Proceedings of the national Academy of Sciences, Vol. 110, No. 41 (October 8, 2013): pg. 16414-16419. DOI.

Brian M. Hoffman
Department of Chemistry, Northwestern University
Evanston, IL
Edwin Antony
Department of Chemistry and Biochemistry
Utah State University
Logan, UT
Lance c. Seefeldt
Department of Chemistry and Biochemistry
Utah State University
Logan, UT

Significance: Biological reduction of dinitrogen (N_2) to ammonia (NH_3) occurs in a select group of bacteria that contain the metalloenzyme nitrogenase. To catalyze this difficult reaction, nitrogenase requires electrons, protons, and ATP. From the earliest studies of nitrogenase, it was realized that ATP hydrolysis is coupled to delivery of electrons and reduction of N_2, yet the order of ATP hydrolysis and electron transfer, which determines the nature of the coupling, was never established. In this work, we establish the order of all the key events during one catalytic cycle of electron delivery in nitrogenase, showing that ATP hydrolysis follows electron transfer. These findings guide future studies aimed at understanding what roles ATP binding and hydrolysis play in the nitrogenase mechanism.

Keywords: nitrogen fixation, metalloprotein

Abstract: The biological reduction of N_2 to NH_3 catalyzed by Mo-dependent nitrogenase requires at least eight rounds of a complex cycle of events associated with ATP-driven electron transfer (ET) from the Fe protein to the catalytic MoFe protein, with each ET coupled to the hydrolysis of two ATP molecules. Although steps within this cycle have been studied for decades, the nature of the coupling between ATP hydrolysis and ET, in particular the order of ET and ATP hydrolysis, has been elusive. Here, we have measured first-order rate constants for each key step in the reaction sequence, including direct measurement of the ATP hydrolysis rate constant: k_{ATP} = 70 s^{-1}, 25 °C. Comparison of the rate constants establishes that the reaction sequence involves four sequential steps: (*i*) conformationally gated ET (k_{ET} = 140 s^{-1}, 25 °C), (*ii*) ATP hydrolysis (k_{ATP} = 70 s^{-1}, 25 °C), (*iii*) Phosphate release (k_{Pi} = 16 s^{-1}, 25 °C), and (*iv*) Fe protein dissociation from the MoFe protein (k_{diss} = 6 s^{-1}, 25 °C). These findings allow completion of the thermodynamic cycle undergone by the Fe protein, showing that the energy of ATP binding and protein–protein association drive ET, with subsequent ATP

Proceedings of the national Academy of Sciences, Vol. 110, No. 41 (October 8, 2013): pg. 16414-16419. DOI.

hydrolysis and Pi release causing dissociation of the complex between the $Fe^{ox}(ADP)_2$ protein and the reduced MoFe protein.

Biological nitrogen fixation catalyzed by the Mo-dependent nitrogenase has a limiting reaction stoichiometry shown in Eq. **1** (1, 2):

$$N_2 + 8e^- + 16MgATP + 8H^+ \rightarrow 2NH_3 + H_2 + 16MgADP + 16Pi: \quad [1]$$

The ATP-driven reduction of one N_2 with evolution of one H_2 requires a minimum of 8 e^- and the hydrolysis of 16 ATP molecules in a complex cascade of events in which electron transfer (ET) from the nitrogenase Fe protein to the catalytic MoFe protein is coupled to the hydrolysis of two ATP molecules (1, 3, 4). The Fe protein is a homodimer with a single [4Fe–4S] cluster and two nucleotide binding sites, one in each subunit (5). The MoFe protein is an $\alpha_2\beta_2$-tetramer, with each αβ-pair functioning as a catalytic unit that binds an Fe protein (6). Each αβ-unit contains an [8Fe–7S] cluster (abbreviated as P cluster) and a [7Fe–9S–Mo–C–*R*-homocitrate] cluster (abbreviated as FeMo cofactor or M cluster) (6–10). In each ET event, the Fe protein, in the reduced (1+) state with two bound ATP, first associates with the MoFe protein (Fig. 1). In a recent model, termed "deficit spending," it is proposed that this association triggers a two-step ET event (11, 12). The first ET step occurs inside the MoFe protein, involving ET from the P cluster resting state (P^N) to the resting FeMo cofactor (M^N), resulting in an oxidized P cluster (P^{1+}) and a reduced FeMo cofactor (M^R) (12). This ET event is conformationally gated (11) with an apparent first-order rate constant (k_{ET}) between 100 and 140 s^{-1} (11, 12). In the second ET step, an electron is transferred from the Fe protein [4Fe–4S] cluster to the oxidized P^{1+} cluster, resulting in the return of the P cluster to the resting oxidation state (P^N) and an oxidized $[4Fe–4S]^{2+}$ cluster in the Fe protein (12). This second step is fast, having a rate constant greater than 1,700 s^{-1} (12).

Proceedings of the national Academy of Sciences, Vol. 110, No. 41 (October 8, 2013): pg. 16414-16419. DOI.

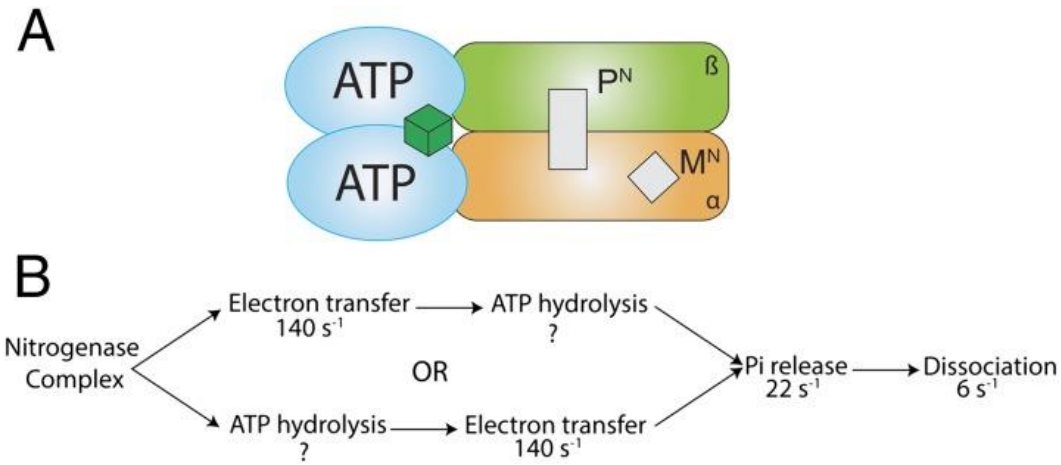

Fig. 1. Order of events in nitrogenase complex. (*A*) Fe protein subunits are shown as two blue ovals (*Left*) with an ATP bound in each subunit and the [4Fe–4S] cluster (green cubane). (*Right*) MoFe protein α-subunit (orange) and β-subunit (green), with the P^N cluster shown as a gray box and the FeMo cofactor (M^N) shown as a gray diamond. (*B*) From left to right, order of events in the nitrogenase ET is shown with rate constants (s^{-1}) displayed where known.

Transfer of one electron from the Fe protein to an αβ-unit of MoFe protein is known to be coupled to the hydrolysis of the two ATP molecules bound to the Fe protein, yielding two ADP and two Pi (2). Following the hydrolysis reaction, the two phosphates (Pi) are released from the protein complex with a first-order rate constant (k_{Pi}) of 22 s^{-1} at 23 °C (13). The last event in the cycle is the release of the oxidized Fe protein with two ADP bound [$Fe^{ox}(ADP)_2$] from the MoFe protein with a rate constant (k_{diss}) of ~6 s^{-1}, the rate-limiting step in catalysis at high electron flux (14). After dissociation from the MoFe protein, the [$Fe^{ox}(ADP)_2$] protein is prepared for a second round of electron delivery by one-electron reduction to [$Fe^{red}(ADP)_2$] and replacement of the two MgADP by MgATP. This cycle is repeated until enough electrons are transferred to the MoFe protein to achieve substrate reduction (15).

Although the energetic coupling between ET and ATP hydrolysis is firmly established (1, 3, 4, 16), the nature of this coupling has remained unresolved: does ATP hydrolysis itself provide the principal energy input for the conformational change(s) that drive ET from Fe protein to the MoFe protein, or, does the bound ATP induce the formation of a reactive, "activated" conformation of the complex, with ET being driven by the free energy of ATP-activated protein–protein binding? These alternatives are characterized by different orders of ET

Proceedings of the national Academy of Sciences, Vol. 110, No. 41 (October 8, 2013): pg. 16414-16419. DOI.

and ATP hydrolysis, but the order has never been established. Some studies have indicated that ATP hydrolysis occurs after ET (13, 17, 18), whereas other studies have suggested just the opposite, namely that ATP hydrolysis occurs before ET (15, 16, 19, 20). One of the reasons for this lack of clarity in the order of these key events is the absence of direct measurement of ATP hydrolysis rates by nitrogenase within a single catalytic cycle. The rate constant for Pi release during one cycle has been measured, thereby establishing a lower limit on the rate constant for ATP hydrolysis (13). However, the rate constant for ATP hydrolysis could be much faster than Pi release, and could be faster than the rate constant for ET.

Here, we have directly measured the rate constant for ATP hydrolysis for a single nitrogenase turnover cycle, as well as measuring the rate constants for each of the other key steps under the same conditions, thereby allowing an unequivocal assignment of the order of events in a single electron-transfer cycle. Establishing the order of events allows a full thermodynamic Fe–protein cycle to be constructed.

Results

ATP Hydrolysis and Pi Release.

The hydrolysis of the 2 ATP bound in the Fe protein to 2 ADP + 2 Pi is initiated during the transient association of the Fe protein with the MoFe protein; ATP hydrolysis is not catalyzed by the Fe protein alone (1). Pre–steady-state rates of ATP hydrolysis during a single Fe–MoFe protein association event have not been reported, although steady-state rates have been reported in several earlier studies, with typical rates ranging from 3,600 to 4,500 $nmol \cdot min^{-1} \cdot (mg\ MoFe\ protein)^{-1}$ (21). These prior steady-state measurements relied on quantification of released ADP or Pi over multiple turnovers, and thus provide little insight into the rate of ATP hydrolysis during the first turnover (21).

Establishing a pre–steady-state rate for ATP hydrolysis is challenging, requiring quantification of ATP consumed and ADP formed on a millisecond time scale. To make this measurement, we used a

Proceedings of the national Academy of Sciences, Vol. 110, No. 41 (October 8, 2013): pg. 16414-16419. DOI.

rapid chemical-quench approach to stop ATP hydrolysis at selected times after initiating the reaction, with an instrument dead-time of 4 ms and time resolution of 1 ms. The ATP and ADP in each quenched solution were quantified by using [^{32}P]ATP (labeled on the α-phosphate) as a tracer. For each sample, ATP was separated from ADP by TLC, with quantification of each nucleotide accomplished by counting of the ^{32}P. Using this approach, it was possible to establish the precise concentration of ADP formed as a function of time after initiating the reaction by rapid mixing (Fig. 2*B*). Over the time range examined (up to 200 ms), the quantity of ADP formed was observed to rise rapidly to a plateau. These data were initially fit to an exponential rise to maximum to get an estimated rate constant, which was found to be noticeably less than k_{ET}, and then the ATP hydrolysis data were fit to the kinetic model described in *Materials and Methods* (Eq. **2**), yielding a rate constant for ATP hydrolysis, k_{ATP} = 70 ± 7 s^{-1} at 25 °C.

Proceedings of the national Academy of Sciences, Vol. 110, No. 41 (October 8, 2013): pg. 16414-16419. DOI.

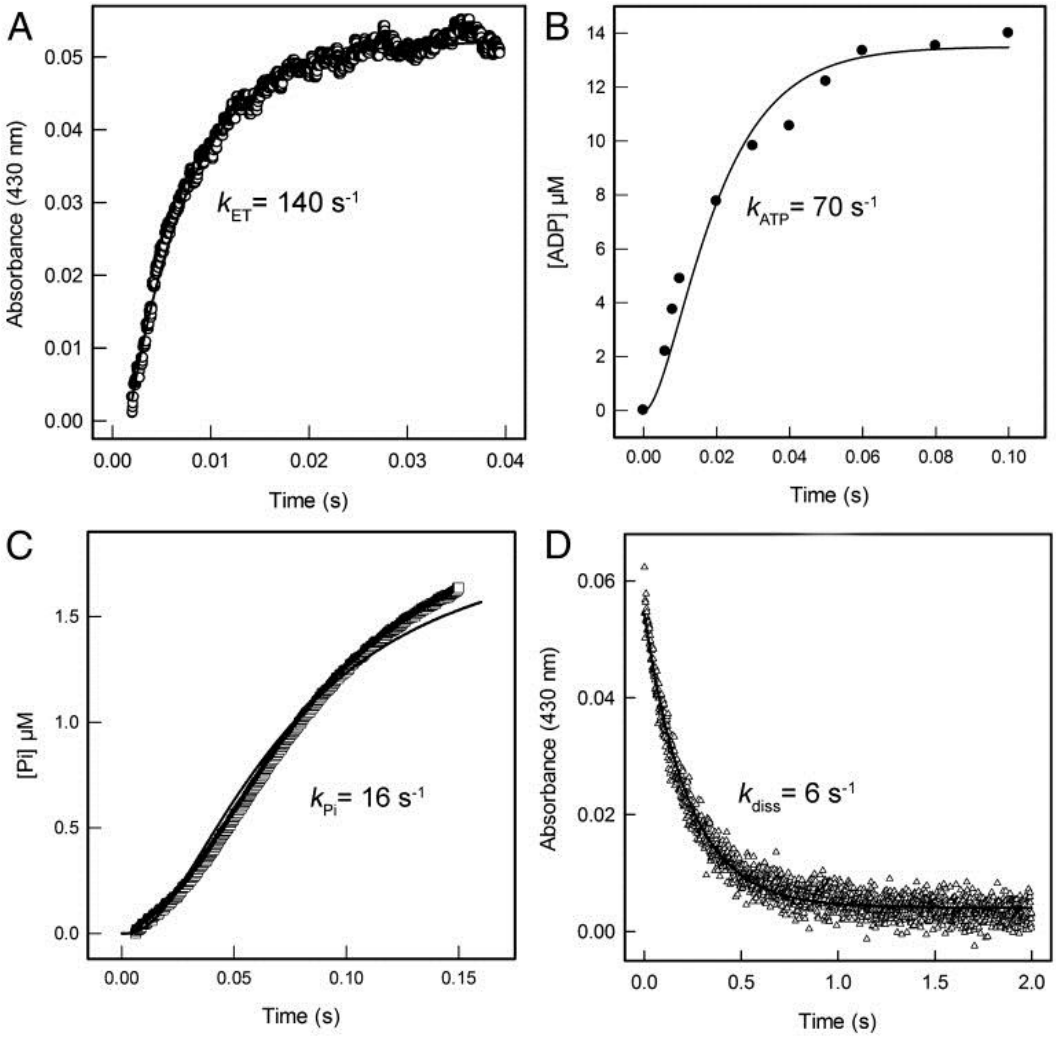

Fig. 2. Kinetics of key nitrogenase catalytic steps. (*A*) ET is monitored as the change in absorbance at 430 nm as a function of time (open circles). The data were fit to the sequential kinetic model (Eq. **2**) (line), with a calculated k_{ET} of 140 s^{-1}. (*B*) ATP hydrolysis is monitored as the formation of α-^{32}P-ADP as a function of time (closed circles). The data were fit to Eq. **2** (line), with a calculated k_{ATP} of 70 s^{-1}. (*C*) Pi release is monitored by the increase in absorbance from Pi binding to the Pi binding protein as a function of time (open square). The data were fit to Eq. **2** (line), with a calculated k_{Pi} of 16 s^{-1}. (*D*) Dissociation of Fe from the MoFe protein is monitored by the decrease in absorbance at 430 nm as a function of time (open triangle). The data were fit to a single-exponential equation (solid line) with a first-order rate constant (k_{diss}) of 6 s^{-1}. All four experiments were carried out at the same experimental conditions at 25 °C.

The rate constant for ATP hydrolysis determined here can be compared with the rate constant for Pi release. In earlier studies, pre–steady-state Pi release was found to have a rate constant (k_{Pi}) of ~22 s^{-1}, roughly threefold less than k_{ATP} (13). The conditions used in the earlier studies were different from the conditions used in the ATP

Proceedings of the national Academy of Sciences, Vol. 110, No. 41 (October 8, 2013): pg. 16414-16419. DOI.

hydrolysis studies reported here, so the Pi release experiment was conducted under the same conditions used for the measurement of ATP hydrolysis. Pi release was detected by binding of the free Pi to a phosphate-binding protein labeled with a fluorescent reporter that shows a sevenfold increase in fluorescence upon Pi binding, thereby allowing real-time monitoring of Pi release using a stopped-flow (SF) fluorometer (Fig. 2*C*) (22). The concentration of Pi released as a function of time was fit to the kinetic model described in *Materials and Methods* (Eq. **2**), yielding a rate constant $k_{Pi} = 16 \pm 1\ s^{-1}$, which is consistent with earlier reports. Fig. 2*C* shows that the kinetic model fits the Pi release data up to almost 150 ms quite satisfactorily, but it was also recognized that at later times the Pi release was more complex due to the achievement of a steady state. As indicated by the result $k_{Pi} < k_{ATP}$, and as visualized when the progress curves for ATP hydrolysis and Pi release are plotted together on a logarithmic time plot (Fig. 3), Pi is not released promptly upon ATP hydrolysis, but rather occurs as a subsequent kinetic step with a detectable delay after ATP hydrolysis.

Proceedings of the national Academy of Sciences, Vol. 110, No. 41 (October 8, 2013): pg. 16414-16419. DOI.

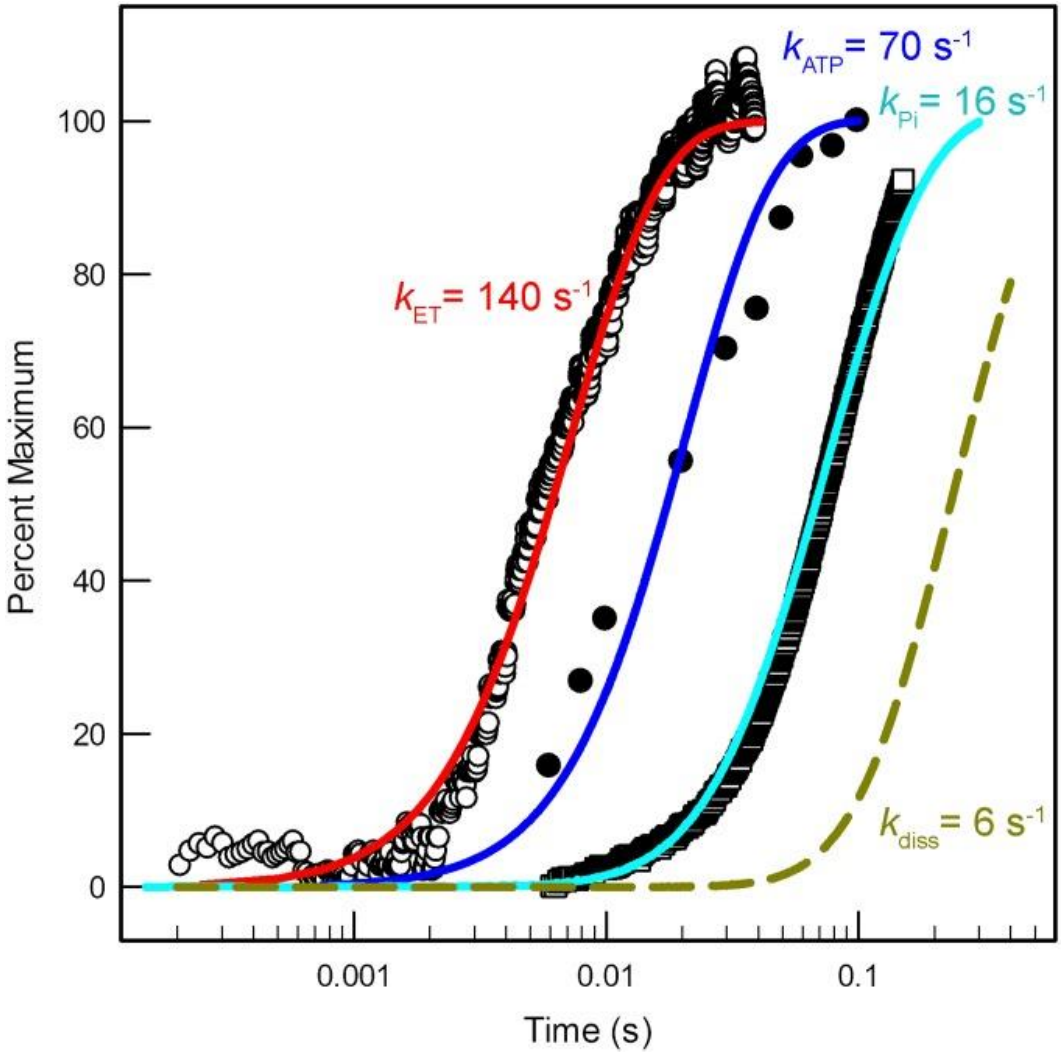

Fig. 3. Time course for key steps in the nitrogenase cycle. The data for ET (○), ATP hydrolysis (●), and Pi release (□) are plotted as a function of the logarithm of time. Each data set was fit to the model in Eq. **2** (solid lines), with the calculated rate constants noted. The protein–protein dissociation is represented by a simulation (dashed green line) generated by using the kinetic model (Eq. **2**), with rate constants fixed at k_{ET} = 140 s^{-1}, k_{ATP} = 70 s^{-1}, and k_{Pi} = 16 s^{-1}.

ATP Hydrolysis Compared with ET.

The rate constant for ET from the Fe protein to the MoFe protein (k_{ET}) has been reported to be between 100 and 150 s^{-1} (23), depending on reaction conditions and the proteins used. This rate constant was reexamined in the present study under identical conditions to the Pi release and ATP hydrolysis measurements. ET is monitored by the absorbance increase that accompanies oxidation of

Proceedings of the national Academy of Sciences, Vol. 110, No. 41 (October 8, 2013): pg. 16414-16419. DOI.

the Fe protein [4Fe–4S] cluster after initiation of the reaction (Fig. 2*A*). Fit of these data to the kinetic model (Eq. **2**) yields an apparent first-order rate constant of k_{ET} = 140 ±10 s^{-1}. This rate constant reflects the oxidation of the Fe protein as an electron is delivered to the MoFe protein, a process recently shown to be gated by protein conformational changes (11). In the deficit-spending model of ET, the observed ET is the last ET event, following conformational gating and ET from the P cluster to FeMo cofactor (12). Thus, the observed first-order rate constant of 140 s^{-1} reflects both protein conformational changes and all ET events.

The rate constant for ATP hydrolysis of k_{ATP} = 70 s^{-1} is half that of the measured ET rate constant, clearly placing ATP hydrolysis as a distinct kinetic step that follows ET. The order of events is visualized by comparing ET, ATP hydrolysis, and Pi release data on a logarithmic time plot (Fig. 3): ET occurs first, followed by ATP hydrolysis, followed by Pi release.

Protein–Protein Dissociation.

Earlier studies have shown that Fe protein dissociation from the MoFe protein is the last event in the cycle, with a first-order rate constant (k_{diss}) ranging from 5 to 10 s^{-1} (14). We directly determined this dissociation rate constant, as described in *Materials and Methods*, under the same conditions as the other measurements (Fig. 2*D*), finding a first-order rate constant of k_{diss} = 6 ±2 s^{-1} from a fit to an exponential of the absorbance change associated with $Fe^{ox}(ADP)_2$ reduction, subsequent to mixing of [$Fe^{ox}(ADP)_2$;MoFe], upon mixing. This value is consistent with protein–protein dissociation being a discrete kinetic step and the last event during the catalytic cycle. The dissociation event is simulated with the kinetic model (Eq. **2**), by fixing the ET, ATP hydrolysis, Pi release, and dissociation rate constants. The simulation (presented as a rise to maximum) clearly places the dissociation as the last event in the series, in a kinetic step distinct from Pi release (Fig. 3).

Proceedings of the national Academy of Sciences, Vol. 110, No. 41 (October 8, 2013): pg. 16414-16419. DOI.

Discussion

Model for Events in the Nitrogenase Cycle.

The measurement of the pre–steady-state rate constant for ATP hydrolysis reported here defines the order of the key events involved in ET within the Fe protein–MoFe protein complex. As is evident in the kinetic progress curves shown in Fig. 3, the order of events is established as: (*i*) ET, (*ii*) ATP hydrolysis, (*iii*) Pi release, followed by (*iv*) dissociation of the Fe protein from the MoFe protein.

The findings of the current study can be combined with earlier findings to construct a model of the key events that occur during one round of Fe protein–MoFe protein association (Fig. 4). The process begins with the formation of a complex between $Fe^{red}(ATP)_2$ and an αβ-catalytic unit of the MoFe protein (Fig. 4, upper left). This association is known to be fast, with a second-order rate constant (k_{assoc}) of 5×10^7 $M^{-1}{\cdot}s^{-1}$ (24). At the concentration of Fe protein used in the present study, the association event is much faster than subsequent events, so all of the measurements described here correspond to first-order, intracomplex steps. Recent studies on the effects of osmotic pressure on the rate of ET have established that following protein–protein association, large-scale (~800 $Å^2$ changes in buried surface) conformational changes within the complex gate subsequent ET events (11). It has been suggested that these conformational changes result in activation of the P cluster to a state (P^{N*}) that transfers an electron to FeMo cofactor, forming the oxidized P cluster (P^{1+}). In this model, subsequent ET from $Fe^{red}(ATP)_2$ to the oxidized P cluster is fast and not gated by protein conformational changes, and generates the final product of intracomplex ET, $Fe^{ox}(ATP)_2$ bound to MoFe protein containing a resting P cluster and one-electron reduced FeMo cofactor (M^R). The overall rate constant for the multiple steps in the ET process is 140 s^{-1} (12).

Proceedings of the national Academy of Sciences, Vol. 110, No. 41 (October 8, 2013): pg. 16414-16419. DOI.

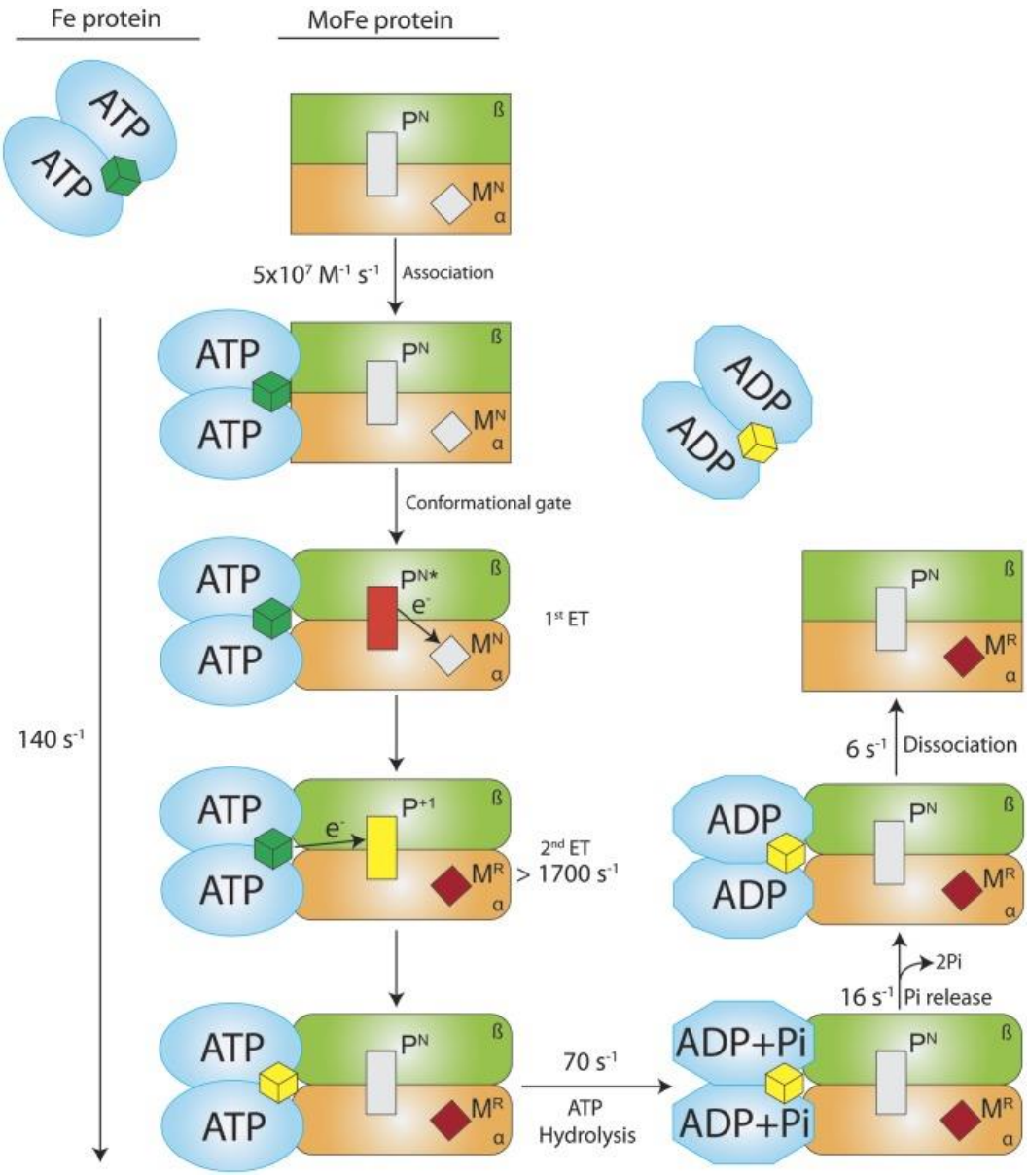

Fig. 4.
Model of nitrogenase order of events. Shown is the Fe protein (blue ovals) with the [4Fe–4S] cluster in the 1+ (dark green cube) or 2+ (yellow cube) oxidation state. The MoFe protein (α-subunit orange and β-subunit green) with the P cluster (rectangle, gray P^N, red activated P^{N*}, and yellow P^{+1} state) and the M cluster (diamond, gray M^N and maroon M^R state). The reaction sequence starts at top left with the association of the Fe protein with the MoFe protein and ends at top right with the dissociation of the oxidized Fe protein from the reduced MoFe protein. First-order rate constant (k, s^{-1}) values for 25 °C are shown. Conformational changes in the Fe protein and MoFe protein are denoted by changes in shape of the ovals or rectangles.

As established here, hydrolysis of the two ATP molecules to ADP and Pi occurs as a distinct kinetic step that follows this ET process.

Proceedings of the national Academy of Sciences, Vol. 110, No. 41 (October 8, 2013): pg. 16414-16419. DOI.

Data shown in Fig. 3 further establish that Pi is not released from the protein–protein complex immediately upon ATP hydrolysis, but Pi is released in a distinct, subsequent step. It seems reasonable to conclude that upon ATP hydrolysis, the complex undergoes conformational changes, although the extent of such changes has not been established. Likewise, it seems reasonable that the release of Pi is accompanied by additional protein conformational changes, but again such changes have not been measured directly.

The final step in the ET process is the release of the $Fe^{ox}(ADP)_2$ from the one-electron reduced MoFe protein (Fig. 4) in a process that is not synchronous with Pi release, but follows as a discrete step with a rate constant of 6 s^{-1}, as has been established in earlier studies (1, 13, 14). The MoFe protein that contains a one-electron reduced FeMo cofactor is then free to be reduced additional times by repeating the process presented in Fig. 4, beginning with the binding of a second $Fe^{red}(ATP)_2$ (15). The released $Fe^{ox}(ADP)_2$ is ready to be returned to the $Fe^{red}(ADP)_2$ state by reduction of its $[4Fe–4S]^{2+}$ cluster reduced back to the 1+ oxidation state, and replacement of ADP by ATP.

The Fe–Protein Cycle.

By revealing that intracomplex $Fe^{red}(ATP)_2 \rightarrow$ MoFe protein ET is followed by ATP hydrolysis (Fig. 4), this work also completes the overall Fe–protein cycle, first formulated by Lowe and Thorneley to summarize the steps undergone by the Fe protein as it delivers an electron to the MoFe protein (1, 17). Fig. 5 presents the key Fe protein reactions formulated as a thermodynamic cycle. The cycle begins with free $Fe^{ox}(ADP)_2$ (Fig. 5, upper right), the final form of Fe protein at the end of a previous ET cycle, and ends with a return to this state upon completion of the cycle. Fig. 5 is further annotated to emphasize the function of the Fe protein as a nucleotide switch (25, 26) that uses ATP binding/hydrolysis to transport an electron from an electron source/reductant to the MoFe protein. Viewed in this way, Fig. 5 introduces a correspondence of the thermodynamic cycle for ATP-dependent electron transport by the Fe protein with the thermodynamic cycle for ATP-dependent substrate export by ATP-binding cassette (ABC) transporters (27–30).

Proceedings of the national Academy of Sciences, Vol. 110, No. 41 (October 8, 2013): pg. 16414-16419. DOI.

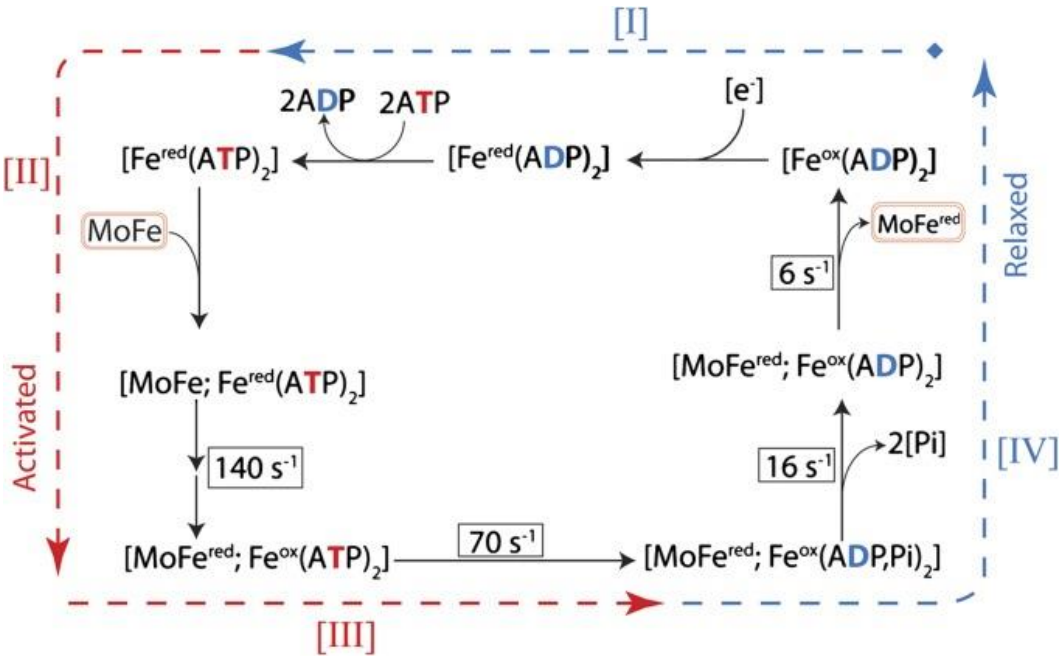

Fig. 5. Thermodynamic Fe–protein cycle. Drawn with a focus on Fe protein electron transport to MoFe protein, it can be viewed as starting at upper right. $MoFe^{red}$ represents reduced MoFe protein. Dashed arrows and notation that surround the cycle refer to analogy with ABC exporter thermodynamic cycle.

The Fe–protein cycle of Fig. 5 (top, right to left) begins with the reduction of $Fe^{ox}(ADP)_2$ to $Fe^{red}(ADP)_2$, which triggers rapid replacement of the 2 ADP by 2 ATP (1, 17). The structure of the Fe protein undergoes major changes upon ATP binding, leading to numerous changes in its properties. However, historically, interest has focused on an ~−120-mV change in the reduction potential of the [4Fe–4S] cluster of nucleotide-free Fe protein upon ATP binding, and the possibility that this change in potential is central to initiating the transfer of an electron to MoFe protein. Although the more negative midpoint potential would favor ET (1), for present purposes note (Fig. 5) that the second step in the thermodynamic Fe–protein cycle is not ATP binding to free Fe protein, but replacement of bound ADP by ATP. Namely, the free Fe^{red} does not appear in the thermodynamic cycle regardless of the mechanistic details of the nucleotide interchange. In fact, the reduction potentials of $Fe^{ox}(ADP)_2$ to $Fe^{red}(ADP)_2$ are the same (31). As a result, ATP/ADP exchange is isopotential, and so the potential lowering upon nucleotide binding cannot contribute to the thermodynamic coupling between ET and ATP binding and hydrolysis.

Proceedings of the national Academy of Sciences, Vol. 110, No. 41 (October 8, 2013): pg. 16414-16419. DOI.

The MoFe protein catalytic unit next binds to $Fe^{red}(ATP)_2$ to form the ET-active [$Fe^{red}(ATP)_2$:MoFe] complex (Fig. 5, down arrow on the left) in a process that changes the Fe protein reduction potential by ~−200 mV (32), presumably through desolvation of its negatively charged [4Fe–4S] cluster (33), thereby preparing the [$Fe^{red}(ATP)_2$;MoFe] complex for interprotein transport of the electron via gated, deficit-spending ET, ATP hydrolysis, Pi release, and subsequent complex dissociation. In the absence of a known ordering of these steps, two alternative proposals have been considered to explain the coupling of ET to ATP binding and hydrolysis. In one, ATP hydrolysis itself provides the principal energy input for the conformational change(s) that drive Fe^{red} → MoFe protein ET; in the other, the bound ATP induces the formation of a reactive, activated conformation of the complex, and it is the free energy of ATP-activated protein-protein binding that drives ET. The present measurements of the rate constants for all of the key steps discriminate between these two alternatives, and in doing so shed further light on the energy transduction through ATP hydrolysis: (*i*) That the ATP hydrolysis is temporally decoupled from and follows ET. Fig. 3 shows that ET is not driven by the free energy of ATP hydrolysis, and that it must be the ATP-dependent free energy of protein–protein binding that drives ET. (*ii*) ATP hydrolysis and Pi release occur as temporally separated steps, both of which precede the dissociation of the product [$Fe^{ox}(ADP)_2$;$MoFe^{red}$] complex (Fig. 4) (13). This demonstrates that both hydrolysis and Pi release are required to completely relax the conformationally activated complex, thereby inducing dissociation of the Fe protein from the reduced MoFe and completing the cycle. A similar sequence of steps was incorporated in the detailed thermodynamic analysis of nitrogenase ET and ATP hydrolysis by Kurnikov et al. (33). They showed that the contribution to the free energy for ET that is derived from formation of the [$Fe^{red}(ATP)_2$;MoFe] complex becomes a stabilization free energy for binding of $MoFe^{red}$ to $Fe^{ox}(ATP)_2$, and that subsequent ATP hydrolysis and Pi release is required to relax the complex and drive the two proteins apart.

Viewed in this way, the Fe protein thermodynamic cycle is analogous to the four-step thermodynamic cycle of the ABC transmembrane substrate transporters, in particular the exporter subclass (27–30). These transporters catalyze substrate transport by a process dependent on conformational changes driven by ATP binding,

Proceedings of the national Academy of Sciences, Vol. 110, No. 41 (October 8, 2013): pg. 16414-16419. DOI.

with the system being reset for another cycle by ATP hydrolysis. The ABC trans(ex)porter cycle begins with binding of the substrate to the protein, which triggers ATP binding (Step I); in nitrogenase the analogous step is electron binding by $Fe^{ox}(ADP)_2$ protein, namely reduction to $Fe^{red}(ADP)_2$, followed by exchange of ADP by ATP. In the transporters, ATP binding free energy drives a sequence of conformational changes that results in an activated state that undergoes transmembrane substrate transport (Step II); in nitrogenase, ATP binding free energy drives the formation of an activated $[Fe^{red}(ATP)_2;MoFe]$ complex that undergoes deficit-spending $Fe^{red} \rightarrow$ MoFe electron transport. In the transporters, ATP hydrolysis to ADP and subsequent Pi release (Step III) elicit conformational relaxation (Step IV), thereby "resetting" the transporter for another catalytic cycle; in nitrogenase, ATP hydrolysis and subsequent Pi release relax the tightly bound $[Fe^{ox}(ATP)_2;MoFe^{red}]$ complex, resulting in dissociation of the reduced MoFe protein (33), leaving the $Fe^{ox}(ADP)_2$ protein ready for another Fe–protein cycle. Thus, the concept of Fe protein as a nucleotide switch must be expanded to include the idea that the Fe protein–MoFe protein complex toggles through two conformational states–activated to achieve ET, and relaxed—following ATP hydrolysis and Pi release to achieve complex dissociation.

Nucleotide-Dependent Structural Changes.

How do nucleotide-dependent changes in the conformation of the [Fe; MoFe] complex drive ET? The X-ray structures of Fe–MoFe protein complexes with a suite of nucleotides (34), including nucleotide-free, ADP-bound, the ATP analog β-γ-methylene ATP (AMPPCP)-bound, and the ATP-hydrolysis transition state represented by ADP–AlF_4^--bound complex, have suggested progressive changes in the structure of Fe protein accompanied by rearrangement at the protein–protein interface as a function of nucleotide state. We interpreted the osmotic-pressure dependence of the observed $Fe^{red} \rightarrow$ MoFe ET process as reflecting motions of the Fe protein relative to MoFe (11), consistent with the crystallographic demonstration that changes in nucleotide state drive large changes in the buried protein–protein interface area (34). However, it must be that activation for ET

Proceedings of the national Academy of Sciences, Vol. 110, No. 41 (October 8, 2013): pg. 16414-16419. DOI.

includes conformational changes within the MoFe protein that have yet to be observed in crystal structures.

Neither the structure of the complex that binds the ATP analog, AMPPCP, nor that of the complex that binds the analog for the transition state of ATP hydrolysis, ADP–AlF_4^-, shows any significant perturbations within the MoFe protein relative to isolated MoFe protein. However, the ABC-transporter-like mechanism encapsulated in the cycle of Fig. 5 offers a possible resolution to this puzzle. As ATP hydrolysis/Pi release occurs only after ET, and thus only contributes to relaxation of the activated conformational state associated with the ATP complex, there is no requirement that the transition state for ATP hydrolysis be associated with a high-energy state within the MoFe protein.

Two further observations can be considered regarding the absence of changes within the MoFe protein in the structure of the AMPPCP-bound complex: (*i*) AMPPCP in fact is not a truly faithful ATP analog in the nitrogenase system, as shown by the inability to promote proper ET and (*ii*) as the deficit-spending ET process is conformationally gated, it may well be that the anticipated state in which FeMo cofactor and its environs are activated for substrate reduction are only formed by a conformational fluctuation and never exists in high occupancy for trapping and direct characterization.

Summary

By establishing the pre–steady-state rate constant for ATP hydrolysis in nitrogenase catalysis, the order of sequential events in the nitrogenase cycle is established to be (*i*) conformationally gated ET, (*ii*) ATP hydrolysis, (*iii*) Pi release, and finally (*iv*) Fe protein dissociation from the MoFe protein. Establishing this order of events provides insights into the functions of ATP in the nitrogenase mechanism, showing that it is the free energy of ATP binding and protein–protein association that control the ET events, with ATP hydrolysis and Pi release causing dissociation of the reduced MoFe protein from the $Fe^{ox}(ADP)_2$ protein.

Proceedings of the national Academy of Sciences, Vol. 110, No. 41 (October 8, 2013): pg. 16414-16419. DOI.

Materials And Methods

Materials, Protein Purification, and Activity Assays.

All reagents, unless stated otherwise, were purchased from Sigma Aldrich Chemicals. Nitrogenase proteins were expressed in *Azotobacter vinelandii* strain DJ995 (wild-type MoFe protein with His tag), and DJ884 (wild-type Fe protein) as described previously (35). The MoFe protein contained a seven-histidine tag near the carboxyl terminus of the α-subunit allowing purification using the previously described metal affinity chromatography method (35). Fe protein was purified using ion exchange and size-exclusion liquid chromatography methods (35, 36). Both proteins were greater than 95% pure based on SDS–polyacrylamide gel electrophoresis separation followed by Coomassie blue staining. Manipulation of proteins was done in septum-sealed serum vials under argon atmosphere. All transfers of gases and liquids were done using gastight syringes.

SF Spectrophotometry and the Oxidation of Fe Protein.

SF spectrophotometry was performed at 25 °C with a Hi-Tech SF61 SF UV-visible spectrophotometer equipped with data acquisition software. The SF unit of the spectrophotometer was housed inside a nitrogen-filled glove box (< 5 ppm O_2). The temperature during the experiments was controlled by a circulating water bath housed outside the glove box (18). In these experiments, 75 μM Fe and 20 μM MoFe protein were contained in one drive syringe whereas the other syringe contained 18 mM $MgCl_2$ and 10 mM ATP. Both syringes contained buffer [100 mM Hepes (pH 7.4) and 10 mM sodium dithionite]. Primary ET from the Fe protein to the MoFe protein was monitored by an increase in absorbance at 430 nm that occurs as the [4Fe–4S] cluster of the Fe protein becomes oxidized during turnover within the [$Fe^{red}(ATP)_2$;MoFe] complex.

The data were fit using KinTech Explorer (KinTek Corp.) to a sequential A → B → C → D → E kinetic model (Eq. **2**).

Proceedings of the national Academy of Sciences, Vol. 110, No. 41 (October 8, 2013): pg. 16414-16419. DOI.

$$\left[\mathrm{Fe^{red}(ATP)_2;MoFe}\right] \underrightarrow{k_{\mathrm{ET}}} \left[\mathrm{Fe^{OX}(ATP)_2;MoFe^{red}}\right] \underrightarrow{k_{\mathrm{ATP}}} \left[\mathrm{Fe^{OX}(ADP,Pi)_2;MoFe^{red}}\right] \underrightarrow{k_{\mathrm{Pi}}} \left[\mathrm{Fe^{OX}(ADP)_2;MoFe^{red}}\right] + 2\mathrm{Pi} \underrightarrow{k_{\mathrm{diss}}} \left[\mathrm{Fe^{OX}(ADP)_2}\right] + \left[\mathrm{MoFe^{red}}\right]$$

[2]

In this model, k_{ET}, k_{ATP}, k_{Pi}, and k_{diss} are the rate constants for ET, ATP hydrolysis, Pi release, and $[Fe^{ox}(ADP)_2;MoFe]$ complex dissociation, respectively. All steps of the ET process can be taken as irreversible except for ATP hydrolysis, and here the rate constant for the reverse reaction is so low that the reverse process can be ignored in the present experiments (1, 17). As a result the sequential model of Eq. **2** is appropriate (in the fitting process all reverse rate constants are set to a value of zero). To fit the ET data, the other rate constants were fixed at k_{ATP} = 70 s^{-1}, k_{Pi} = 16 s^{-1}, and k_{diss} = 6 s^{-1}.

Quench-Flow Studies for ATP Hydrolysis.

Pre–steady-state ATP hydrolysis assays were performed at 25 °C on a rapid chemical quench-flow instrument (KinTek Corp.) housed in a nitrogen-filled glove box (< 5 ppm O_2). An 18-μL volume of 10 μM MoFe and 20 μM Fe (syringe A) was mixed with an 18-μL volume of 1 mM ATP with [α-^{32}P]ATP (1.5 μCi) from syringe B, with varying times of reaction. Reactions were rapidly quenched with 45 μL 0.5 M EDTA added from syringe C. Aliquots (0.9 μL) of the quenched reaction were spotted onto a TLC plate and developed in 0.6 M potassium Pi buffer, pH 3.4, for 45 min. The [α-^{32}P]ATP and the [α-^{32}P]ADP were detected with a Storm PhosphorImager (Molecular Dynamics) and quantified using the ImageQuant software (Molecular Dynamics). The data were fit to the kinetic model (Eq. **2**), with fixed values of k_{ET} = 140 s^{-1}, k_{Pi} = 16 s^{-1}, and k_{diss} = 6 s^{-1}.

Kinetics of Inorganic Pi Release.

The time course of Pi release was determined in a SF fluorometer (Auto SF-120, KinTek Corp.) using the coumarin (*N*-[2-(1-

Proceedings of the national Academy of Sciences, Vol. 110, No. 41 (October 8, 2013): pg. 16414-16419. DOI.

maleimidyl)ethyl]-7-(diethylamino) coumarin-3-carboxamide) labeled phosphate binding protein assay (22). Briefly, Pi binding to MDCC-PBP results in an increase in fluorescence (13, 22) (λ-excitation = 430 nm, λ-emission >450 nm). The experiments were carried out at 25 °C in SF buffer (0.5 mM sodium dithionite and 25 mM Hepes; pH 7.4). Before each experiment, the SF syringes and flow lines were treated with a Pi mop (SF-buffer with 300 μM 7-methylguanine (7-meG), and 0.2 units/mL purine nucleoside phosphorylase (PNPase) for 15 min to remove contaminating Pi (22) and then rinsed with buffer. Two μM MoFe and 6 μM Fe were rapidly mixed with a solution of 10 μM MDCC-PBP, 20 mM $MgCl_2$ and 2mM ATP and the change in fluorescence was monitored over time. A control time course, conducted without nitrogenase, was used to correct for the presence of contaminating Pi. MDCC-PBP fluorescence enhancement was converted to [Pi] after calibration in the SF using [KH_2PO_4] standards as described (22). The Pi release data were fit to the sequential kinetic model (Eq. **2**) with k_{ET} = 140 s^{-1}, k_{ATP} = 70 s^{-1}, and k_{diss} = 6 s^{-1} fixed.

The Fe Protein–MoFe Protein Dissociation Rate Constant.

The dissociation of the Fe protein from the MoFe protein was determined by following the release of the Fe protein from the MoFe protein in the SF spectrophotometer. $Fe^{ox}(ADP)_2$ is not reduced by dithionite within the [$Fe^{ox}(ADP)_2$;MoFe] complex. Thus, the rate constant for the dissociation of the [$Fe^{ox}(ADP)_2$;MoFe] complex was determined by measuring the decrease in absorbance at 430 nm during the reduction of Fe^{ox} to Fe^{red} by dithionite after $Fe^{ox}(ADP)_2$ dissociates from the MoFe protein (14). Rate constant for dissociation was determined by fitting the data to a single-exponential equation (Eq. **3**):

$$A=e^{-k(diss)t}, \qquad [3]$$

where A is the amplitude of the absorbance change and k_{diss} is the rate constant for dissociation of the complex. Sodium dithionite was removed from the as-isolated MoFe and Fe proteins and exchanged

Proceedings of the national Academy of Sciences, Vol. 110, No. 41 (October 8, 2013): pg. 16414-16419. DOI.

into 50 mM Hepes buffer with 200 mM NaCl, pH 7.4, by passage over a Sephadex G-25 column. Oxidized Fe protein was generated by adding increments of a 25-mM Indigo disulfonate (IDS) solution to the Fe protein until a blue color remained. The excess IDS was removed by passing the sample over a Dowex ion-exchange resin and Sephadex G-25 column equilibrated with 50 mM Hepes buffer, pH 7.4. For each experiment, syringe A contained 40 μM Fe^{ox} protein, 40 μM MoFe protein, 5 mM MgADP in 50 mM Hepes buffer, pH 7.4, and syringe B contained 200 μM Fe^{red} protein, and 20 mM sodium dithionite in 50 mM Hepes buffer, pH 7.4.

Acknowledgments

The phosphate binding protein was a kind gift from Dr. Martin Webb. This work was funded by National Institutes of Health Grants R01-GM59087 (to L.C.S. and D.R.D.) and HL63203 (to B.M.H.).

Footnotes

The authors declare no conflict of interest.

This article is a PNAS Direct Submission.

References

1. Burgess BK, Lowe DJ. Mechanism of molybdenum nitrogenase. Chem Rev. 1996;96(7):2983–3012.
2. Seefeldt LC, Hoffman BM, Dean DR. Mechanism of Mo-dependent nitrogenase. Annu Rev Biochem. 2009;78:701–722.
3. Thorneley RN, Lowe DJ, Eday RR, Miller RW. The coupling of electron transfer in nitrogenase to the hydrolysis of magnesium adenosine triphosphate. Biochem Soc Trans. 1979;7(4):633–636.
4. Hageman RV, Orme-Johnson WH, Burris RH. Role of magnesium adenosine 5′-triphosphate in the hydrogen evolution reaction catalyzed by nitrogenase from *Azotobacter vinelandii*. Biochemistry. 1980;19(11):2333–2342.
5. Georgiadis MM, et al. Crystallographic structure of the nitrogenase iron protein from *Azotobacter vinelandii*. Science. 1992;257(5077):1653–1659.
6. Kim J, Rees DC. Structural models for the metal centers in the nitrogenase molybdenum-iron protein. Science. 1992;257(5077):1677–1682.

7. Chan MK, Kim J, Rees DC. The nitrogenase FeMo-cofactor and P-cluster pair: 2.2 A resolution structures. Science. 1993;260(5109):792–794.
8. Lancaster KM, et al. X-ray emission spectroscopy evidences a central carbon in the nitrogenase iron-molybdenum cofactor. Science. 2011;334(6058):974–977.
9. Spatzal T, et al. Evidence for interstitial carbon in nitrogenase FeMo cofactor. Science. 2011;334(6058):940.
10. Einsle O, et al. Nitrogenase MoFe-protein at 1.16 A resolution: A central ligand in the FeMo-cofactor. Science. 2002;297(5587):1696–1700.
11. Danyal K, Mayweather D, Dean DR, Seefeldt LC, Hoffman BM. Conformational gating of electron transfer from the nitrogenase Fe protein to MoFe protein. J Am Chem Soc. 2010;132(20):6894–6895.
12. Danyal K, Dean DR, Hoffman BM, Seefeldt LC. Electron transfer within nitrogenase: Evidence for a deficit-spending mechanism. Biochemistry. 2011;50(43):9255–9263.
13. Lowe DJ, et al. (1995) Nitrogen fixation: Fundamentals and applications. *Current Plant Science and Biotechnology in Agriculture*, eds Tikhonovich IA, Provorov NA, Romanov VI, Newton WE (Springer, Dordrecht, The Netherlands), pp 103–108.
14. Thorneley RN, Lowe DJ. Nitrogenase of *Klebsiella pneumoniae*. Kinetics of the dissociation of oxidized iron protein from molybdenum-iron protein: Identification of the rate-limiting step for substrate reduction. Biochem J. 1983;215(2):393–403.
15. Hageman RV, Burris RH. Nitrogenase and nitrogenase reductase associate and dissociate with each catalytic cycle. Proc Natl Acad Sci USA. 1978;75(6):2699–2702.
16. Eady RR, Lowe DJ, Thorneley RNF. Nitrogenase of *Klebsiella pneumoniae*: A pre-steady state burst of ATP hydrolysis is coupled to electron transfer between the component proteins. FEBS Lett. 1978;95(2):211–213.
17. Wilson PE, Nyborg AC, Watt GD. Duplication and extension of the Thorneley and Lowe kinetic model for *Klebsiella pneumoniae* nitrogenase catalysis using a MATHEMATICA software platform. Biophys Chem. 2001;91(3):281–304.
18. Lanzilotta WN, Fisher K, Seefeldt LC. Evidence for electron transfer from the nitrogenase iron protein to the molybdenum-iron protein without MgATP hydrolysis: Characterization of a tight protein-protein complex. Biochemistry. 1996;35(22):7188–7196.
19. Imam S, Eady RR. Nitrogenase of *Klebsiella pneumoniae*: Reductant-independent ATP hydrolysis and the effect of pH on the efficiency of coupling of ATP hydrolysis to substrate reduction. FEBS Lett. 1980;110(1):35–38.

Proceedings of the national Academy of Sciences, Vol. 110, No. 41 (October 8, 2013): pg. 16414-16419. DOI.

20. Thorneley RN, Ashby G, Howarth JV, Millar NC, Gutfreund H. A transient-kinetic study of the nitrogenase of *Klebsiella pneumoniae* by stopped-flow calorimetry. Comparison with the myosin ATPase. Biochem J. 1989;264(3):657–661.
21. Ryle MJ, Seefeldt LC. Hydrolysis of nucleoside triphosphates other than ATP by nitrogenase. J Biol Chem. 2000;275(9):6214–6219.
22. Brune M, Hunter JL, Corrie JE, Webb MR. Direct, real-time measurement of rapid inorganic phosphate release using a novel fluorescent probe and its application to actomyosin subfragment 1 ATPase. Biochemistry. 1994;33(27):8262–8271.
23. Fisher K, Lowe DJ, Thorneley RN. *Klebsiella pneumoniae* nitrogenase. The pre-steady-state kinetics of MoFe-protein reduction and hydrogen evolution under conditions of limiting electron flux show that the rates of association with the Fe-protein and electron transfer are independent of the oxidation level of the MoFe-protein. Biochem J. 1991;279(Pt 1):81–85.
24. Lowe DJ, Thorneley RN. The mechanism of *Klebsiella pneumoniae* nitrogenase action. The determination of rate constants required for the simulation of the kinetics of N_2 reduction and H_2 evolution. Biochem J. 1984;224(3):895–901.
25. Rees DC, et al. Structural basis of biological nitrogen fixation. Philos Trans A Math Phys Eng Sci. 2005;363(1829):971–984, discussion 1035–1040.
26. Rees DC, Howard JB. Structural bioenergetics and energy transduction mechanisms. J Mol Biol. 1999;293(2):343–350.
27. Linton KJ, Higgins CF. Structure and function of ABC transporters: The ATP switch provides flexible control. Pflügers Arch - Eur J Physiol. 2007;453(5):555–567.
28. Locher KP. Review. Structure and mechanism of ATP-binding cassette transporters. Philos Trans R Soc Lond B Biol Sci. 2009;364(1514):239–245.
29. Goetz BA, Perozo E, Locher KP. Distinct gate conformations of the ABC transporter BtuCD revealed by electron spin resonance spectroscopy and chemical cross-linking. FEBS Lett. 2009;583(2):266–270.
30. Rees DC, Johnson E, Lewinson O. ABC transporters: The power to change. Nat Rev Mol Cell Biol. 2009;10(3):218–227.
31. Lanzilotta WN, Ryle MJ, Seefeldt LC. Nucleotide hydrolysis and protein conformational changes in *Azotobacter vinelandii* nitrogenase iron protein: Defining the function of aspartate 129. Biochemistry. 1995;34(34):10713–10723.
32. Lanzilotta WN, Seefeldt LC. Changes in the midpoint potentials of the nitrogenase metal centers as a result of iron protein-molybdenum-iron protein complex formation. Biochemistry. 1997;36(42):12976–12983.

33. Kurnikov IV, Charnley AK, Beratan DN. From ATP to electron transfer: Electrostatics and free-energy transduction in nitrogenase. J Phys Chem B. 2001;105(23):5359–5367.
34. Tezcan FA, et al. Nitrogenase complexes: Multiple docking sites for a nucleotide switch protein. Science. 2005;309(5739):1377–1380.
35. Christiansen J, Goodwin PJ, Lanzilotta WN, Seefeldt LC, Dean DR. Catalytic and biophysical properties of a nitrogenase Apo-MoFe protein produced by a *nifB*-deletion mutant of *Azotobacter vinelandii*. Biochemistry. 1998;37(36):12611–12623.
36. Burgess BK, Jacobs DB, Stiefel EI. Large-scale purification of high activity *Azotobacter vinelandII* nitrogenase. Biochim Biophys Acta. 1980;614(1):196–209.